Nanoscale

Accepted Manuscript

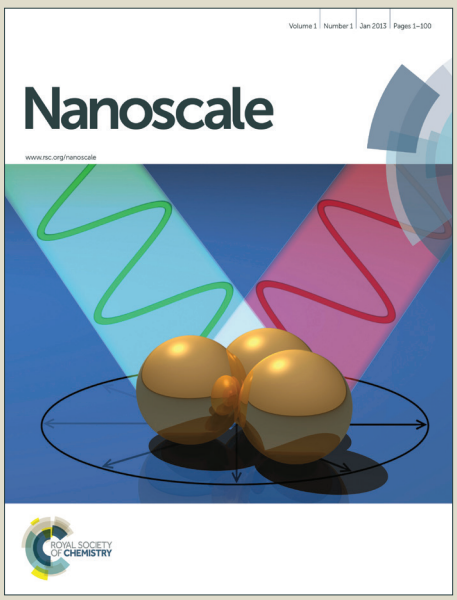

ROYAL SOCIETY OF CHEMISTRY

www.rsc.org/nanoscale

Journal Name

RSCPublishing

ARTICLE

The Comparative Experiments of Graphene Covalently and Physically Binding CdSe Quantum Dots to Enhance the Electron Transport in the Flexible Photovoltaic Devices

Cite this: DOI: 10.1039/x0xx00000x

Received 00th January 2012,
Accepted 00th January 2012

DOI: 10.1039/x0xx00000x

www.rsc.org/

Mi-Hee Jung,*[a] and Moo-Jung Chu [a]

In this research, we prepared composite films via covalent coupling of CdSe quantum dots (QDs) to graphene through the directly binding aryl radical to the graphene surface. To compare the carrier transport with the CdSe aryl binding graphene film, we prepared CdSe pyridine capping graphene films through the pi-pi interaction of the noncovalent bond between the graphene and pyridine molecule. The photovoltaic devices were fabricated from the two hybrid films using the electrophoretic deposition method on flexible substrates. Even though two hybrid films have the same amount of QDs and graphene, time-resolved fluorescence emission decay results show that the emission lifetime of CdSe aryl groups binding graphene film is significantly shorter than that of the pyridine capping CdSe-graphene. The quantum efficiency and photocurrent density of device fabricated from CdSe aryl binding graphene were also higher than that of device fabricated from pyridine capping CdSe-graphene. These results indicated that the carrier transport of the QDs-graphene system is not related to the additive effect from the CdSe and graphene components but rather a result of the unique interactions between the graphene and QDs. We could expect that these results can be useful to design QDs-graphene composite materials, which was applied in photovoltaic devices.

1. INTRODUCTION

The Dye-sensitized solar cells (DSSCs) are regarded as a promising alternative to conventional solid-state semiconductor solar cells. DSSCs are cost effective, easily manufactured, and can be readily shaped with flexible substrates to satisfy the demands of various applications. Evolving from DSSCs, a power conversion efficiency (PCE) of DSSCs as high as 12% has been achieved using porphyrin-sensitized mosophorous TiO_2 photoanode and cobalt redox electrolyte;[1] whereas, recent reports of solid state DSSCs based on perovskite $CH_3NH_3PbI_3$ sensitizer family have exceeded PCE of 15%,[2] promising further breakthrough in this field study. To meet the demand of clean energy from solar cell with high efficiency, quantum dots based solar cells will be also expected to play a leading role in this revolution owing to their potential properties. Instead of using organic dyes, researchers have achieved the sensitization of TiO_2 nanoporous electrodes by modifying quantum dots (QDs) of low bandgap materials, such as CdS,[3] CdSe,[4] CdTe,[5] PbS,[6] and InAs[7] which absorb light in the visible region. Semiconductor QDs offer significant advantages over dyes. QDs can match the solar spectrum better than dyes because their absorption spectrum can be tuned to the particle size.[8] In addition, QDs have recently been shown to generate multiple excitons, which can improve the device efficiency.[9] However, despite the advantages of using QDs as a sensitizer, QD cells are less efficient than dye cells[10] due to fast recombination of electron-hole pairs. Fast capture of electrons at the QD interface remains a major challenge for efficient harvesting of light energy. This issue is of great importance in relation to exploiting multiple charge carrier generation for photocurrent generation. The strategy of encapsulating QDs with an electron acceptor shell or decorating them on a semiconductor nanotube assembly can provide new ways to enhance the capture and transport of photogenerated electrons. Fullerenes exhibit rich photochemistry and act as shuttles in photochemical solar cells. C_{60} and its derivatives are widely used to capture and transport electrons in organic solar cells. In a previous study a CdSe QDs and C_{60} mixture was dropcast on a conducting surface for the purpose of demonstrating photovoltaic performance.[11] However, poor interaction between the two components resulted in relatively poor photocurrent generation. In the meanwhile, on the basis of their unique electrical and electronic properties, a wide electrochemical stability window, and high surface area,

carbon nanostructures have been employed in many applications, such as the use of single wall carbon nanotube (SWCNT) assemblies for energy conversion devices.[12,13] However, it is typically very difficult to achieve a uniform QDs distribution because SWCNTs always exist in a bundle form in solution as a result of their hydrophilicity and the size of QDs is in a similar range as the diameters of the SWCNT bundles, thus making stacking difficult. Such a better distribution of QDs on graphene appears to be favorable for the performance improvement of photovoltaic devices.[14] Graphene, a new class of 2D carbon structures, has demonstrated unique properties, such as high mobility and saturation velocity for both electrons and holes. The most important characteristic of graphene is its work function, 4.7 eV~ 4.9 eV, which is similar to that of gold and enables possible ohmic hole injection into most organic semiconductors with comparable HOMO energy levels. The efficiency of graphene in capturing and transporting electrons from CdSe QDs is superior to other carbon nanostructure based cells reported elsewhere.[11,15] This conclusion is in agreement with earlier work on captured electrons from H2P-C60 systems.[16] The ability to capture electrons from QDs thus paves the way for their use in photovoltaic applications. Graphene/quantum dots (GQ) hybrid nanostructures are expected to facilitate charge transfer to two-dimensional (2D) structures, as well as efficient carrier transport.[17] The chemical formation of carbon-carbon bonds offer an alternative approach to the electronic properties of graphene; the transformation of the carbon centers form sp^2 to sp^3 introduces a barrier to electron flow by opening a band gap and allows the generation of insulating and semiconducting regions in graphene sheet. The prototype chemistry when applied to carbon nanotubes allowed both covalent and ionic chemical modification of the electronic structure;[18] thus the covalent attachment of dichlorocarbene has been shown to transform the metallic SWCNT into semiconductors.[19] The reduction of diazonium salts has been widely utilized for grafting aryl groups to the surface of sp^2-hybridized carbon materials including glassy carbon,[20] HOPG,[21] and carbon nanotubes,[22] as well as to the sp^3-bonded carbon atoms of diamond.[23]

In this research, GQ hybrid materials were synthesized and assembled as the photoanode of solar cells through the covalent binding ligand. To prepare the GQ hybrid composite, we present a simple, covalent method for anchoring CdSe QDs onto a graphene sheet through a ligand-exchange approach. An innovative approach is presented herein based on modification of prepared trioctylphosphine oxide (TOPO) capped CdSe QDs with a bifunctional group, 4-aminothiophenol (AmTP) and subsequent a diazotization reaction. The diazotized CdSe-AmTP QDs were reacted with graphene on the flexible substrates. The surface modification of graphene with CdSe aryl group was achieved through the spontaneous reaction of the diazonium salt with the graphene layer. The reaction is due to spontaneous electron transfer from the graphene layer and its substrate to the diazonium salt. The aryl group functioned as a short, covalent linker between the QDs and graphene and allowed more efficient carrier transfer through the assemblies without deleteriously altering electronic structures, thus providing a simple methodology to design robust GQ films on transparent conducting electrodes. The possibility of CdSe realizing graphene films opens new ways to replace the dye/TiO_2 system in DSSCs.

2. EXPERIMENTAL SECTION

Trioctylphosphine oxide (TOPO)-capped CdSe QDs were synthesized by a solution-chemical route developed by Peng and co-workers.[24] To exchange TOPO capped CdSe QDs with AmTP, The ligand exchange reactions were performed by adding a solution of TOPO capped CdSe nanoparticles in toluene to a boiling solution of 5-10 equivalents of AmTP in the same solvent. For instance, CdSe-AmTP were obtained by adding 4 mg of CdSe nanoparticles dissolved in 2.0 ml of toluene to a boiling solution of 5-10 mole equivalents of AmTP ligand in toluene. After 5 minutes, the product precipitated as a red brown solid, which was isolated by centrifugation, washed with toluene to remove excess ligand, and dried in vacuo. These nanoparticles can readily be resuspended in THF or DMF.[25] AmTP modified CdSe QDs was diazotized with the following the way. 0.268 g (1 mmol) of CdS-AmTP was dissolved in 10 ml of ethanol. To the solution, 0.069 g (1 mmol) of $NaNO_2$ in 10 ml water was added drop-wise, and then, a few drops of concentrated hydrochloric acid (HCl) were added. After adding $NaNO_2$ solution, reactants were mixed together by stirring. The temperature of the reaction mixture was kept between 0-5 ℃ for 20 minutes. The ethanolic solution of diazotized CdS-AmTP became immediately yellow after adding concentrated HCl. The mixture was kept on ice and used in coupling reaction, quickly.[25]

To compare with the CdSe aryl radical functionalized graphene, the TOPO QDs were surface ligand exchanged with pyridine by stirring overnight with mild heating (90 ^oC). An excess of pyridine molecules (over 10 × the caculated mol % of surface atoms) was used to complete the surface exchange. The pyridine capped CdSe were precipitated using hexane. Pyridine capped CdSe were then mixed with graphene power and sonicated until optically clear solution obtained (bath type sonicator, 40 kHz, 5-10 min).[26]

The GO was synthesized according to the modification of Hummers' methods and exfoliated and dispersed in DI water.[27,28] The graphene was prepared via the chemical reduction using the hydrazine.[29] The reduced graphene was washed with ethanol several times and dispersed in ethanol. The graphene solution was mixed with diazonium and pyridine capped CdSe typically consisting of 50 μL of 9.0×10^{-6} M CdSe QDs in toluene and 30 μL of 0.5 mg/mL graphene in ethanol, combined in a 0.8:1.0 mixture of toluene/acetonitrile.[30] We kept the same amount of the loaded CdSe QDs on graphene in both hybrid films.

The CdSe−graphene films were created by electrophoretic deposition. Briefly, two ITO/PET flexible electrodes were held apart at a constant distance of 4 mm in the electrophoretic deposition (EPD) while a potential of 50 V was applied. EPD

cycles consisted of 1 min deposition periods followed by remixing. The obtained film thickness is 200 nm.

To prepare Pt counter-electrodes, we coated the ITO/PET flexible substrate with Pt with the sputtering process. The GQ composite deposited electrode and the Pt counter-electrode were assembled into a sealed sandwich-type cell by heating with a hot melt of a 50 μm thick Surlyn polymer film (Surlyn, Dupont 1702). The electrolyte consists of Na_2S (0.5 M), S (2 M) and KCl (0.2 M) in a methanol/water (7:3 by volume) solution.[31] The photocurrent (Jsc) and photovoltage (Voc) of the DSSCs were measured with an active area of 0.15-0.25 cm^2 using simulated solar light at AM 1.5 that was produced by a 1000 W xenon lamp (Oriel, 91193). Its irradiant power was adjusted with respect to a Si reference solar cell (Fraunhofer Institute for Solar Energy System: Mono-Si + KG filter) to approximately one-sun light intensity (100 mW/cm^2). Incident photon-to-current efficiency (IPCE) was measured using a system designed by PV measurement. A 12 W halogen lamp was applied as a light source for the monochromatic beam. For its calibration, a silicon photodiode (NIST-calibrated photodiode G425) was used. IPCE data was obtained at a low chopping speed of 5 Hz, and the quantum efficiency was detected by a lock-in amplifier. HR-TEM images were obtained with a JEM-2100F (JEOL Ltd., Japan). The optical-absorption spectra of the QDs solution were measured with an ultraviolet-visible-near infrared (UV-vis-NIR) spectrophotometer (Shimadzu UV-1601). Atomic force microscopy (AFM) measurements were carried out on a Multimode XE-100 instrument (PSIA Inc.) operating in tapping mode with silicon cantilevers (resonance frequency in the range of 204-259 kHz, an integrated Si tip with a typical radius of 10 nm curvature). Photoluminescence (PL) measurements of QDs and GQ were performed using the 325 nm line of a He-Cd laser as the excitation source at room temperature. Time-resolved fluorescence spectroscopy was measured by the time correlated single photon counting (TCSPC) using a Micro-Time 200 (PicoQuant GmbH) spectrofluorimeter equipped with a 470 nm diode (full width at half maximum, 96 ps) with a 40 MHz repetition rate. Infrared spectroscopy (IR) has been used to determine the functional groups on the surface of dots and also the formation of metal sulphur bonds and linkage between individual objects. IR spectra were measured on a Nicolet 5700 FT-IR spectrometer in the wave number region 400-4000 cm^{-1}. Raman spectra were obtained with a high resolution dispersive raman microscope (Horiba Jobin Yvon, France). The 514.5 nm radiation from a 40 mW air-cooled argon ion laser was used as the exciting source. The laser power at the sample position was 2.0 mW for graphene and QDs modified graphene. Data acquisition was the result of five 30 s accumulation for sample.
The photocurrent response of ON-OFF illumination was meaured on a ZAHNER CIMPS system. A stationary DC voltage and a concurrent sinusoidal modulated AC voltage were imposed on a green LED, which gave out a green irradiance with a maximum wavelength at 525 nm and 100 W/cm^2. The LED was controlled by a potentiostatic feedback loop. The intensity modulated photovoltage spectroscopy (IMVS) and intensity modulated photocurrent spectroscopy (IMPS) measurements were performed on a ZAHNER CIMPS system. A stationary DC voltage and a concurrent sinusoidal modulated AC voltage were imposed on a green LED, which gave out a green irradiance with a maximum wavelength at 525 nm. The LED was controlled by a potentiostatic feedback loop. The selected AC amplitude ranged from 5% to 15% of the stationary DC value. The transfer functions of IMPS and IMVS were determined by correlating the system response with the actual stimulation signal. The potential applied to the testing cell was controlled by a potentiostat unit. IMPS measurement was carried out under short-circuit condition while IMVS measurement was carried out under open-circuit condition. The measured short circuit photocurrent efficiency ($\Phi ext(\omega)$) of IMPS and the real and imaginary parts of modulated photovoltage ΔVoc of IMVS were fitted by using the Levenberg-Marquardt algorithm.

3. RESULTS AND DISCUSSION

We propose a synthetic strategy for QDs and graphene covalently binding process, as shown in Scheme 1. The TOPO ligand is commonly used to cap and passivate the surface of CdSe quantum dots for a variety of reasons: it coordinates the surface cadmium atoms, forms a protective layer against sintering, provides solubility, and maintains good optical properties. In this work, QDs surface coatings were modified in order to combine with the graphene under suitable conditions.

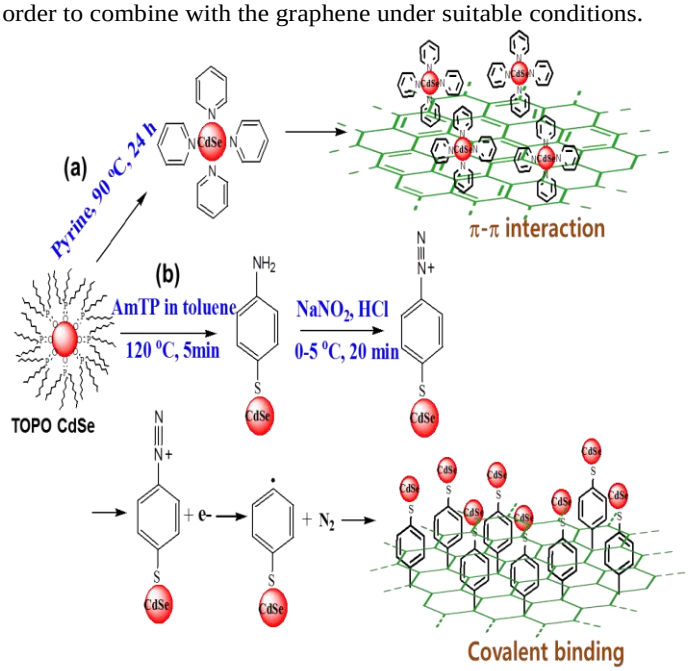

Scheme 1. Schematic illustration of (a) the combination of pyridine capped QDs with graphene using the noncovalent approach (π-π interaction) to fabricate the QDs-graphene films. (b) The grafting process of aryl diazonium cation functionlized CdSe to graphene via reduction of CdSe diazonium salt: The CdSe aryl diazonium cation accepts one electron from the substrate and forms an aryl radical through the release of a nitrogen molecule. The aryl radical can then covalently react with the graphene surface.

The capping agent from the initial synthesis, TOPO, were substantially replaced by a bifunctional group, AmTP, by a ligand exchange reaction. The reaction was performed by adding a solution of TOPO capped CdSe in toluene to a boiling solution of 0.1 M AmTP in the same solvent. The head of bifunctional molecules (usually sulfur) predominantly attaches to the soft nanoparticles, and the tail possessing a terminal reactive functional group is hence available for further reaction. We can replace more than 90% of TOPO with AmTP. The AmTP functionalized CdSe was confirmed by FT-IR spectroscopy; the spectrum of AmTP functionalized QDs exhibits new bands at 3333 and 3426 cm^{-1}, which fall within the range of the symmetric and asymmetric stretching modes of the NH_2 group (Figure 1).[25] Subsequently, diazonium functionalized CdSe were prepared from a diazotization reaction of an aromatic primary amine of AmTP by converting it to a diazoium compound. The diazonium functionalized CdSe was identified with N≡N stretching frequency at 2277 cm^{-1} (Figure 1).[32] Aryl diazonium salts are known to react with olefins.[33] In solution-phase reactions, diazonium salt decomposition is typically catalyzed by a metal salt such as

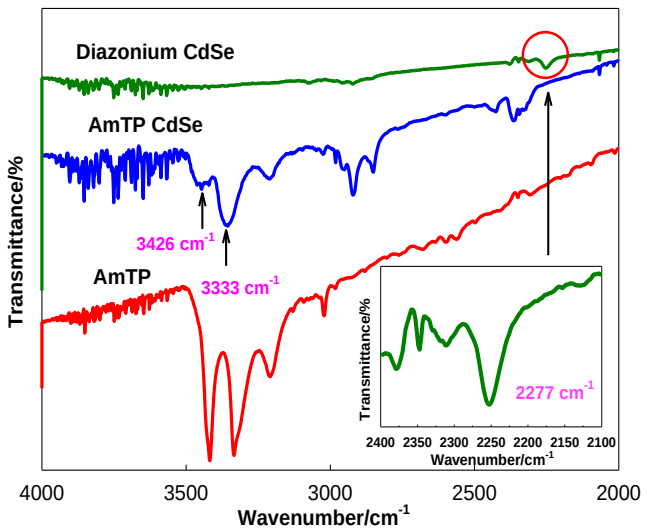

Figure 1. IR spectra of AmTP, AmTP functionalized CdSe nanoparticles and CdSe diazonium salt nanoparticles after diazotization. Spectrum of CdSe diazonium salt nanoparticles shows diazonium (-N≡N-) stretching frequency at 2277 cm^{-1}.

copper chloride, giving a reactive aryl radical. This type of chemistry has been successfully applied to the modification of carbon surface via grafting of electrochemically reduced aryl diazonium salt. The diazonium capped CdSe QDs has a positive charge due to the diazonium cation. Reduction gives an aryl radical that covalently attaches to the graphene surface, as shown in Scheme 1b. Therefore, the AmTP CdSe was linked to the graphene by covalent attachment of aryl groups to the basal carbon atoms. Diazonium cation functioned QDs multiple roles, simultaneously. First, the benzene diazonium capped CdSe QDs were assembled much more effectively onto the graphene compared to the original TOPO-capped QDs, thereby meeting the requirement to produce the composite of graphene and QDs. Second is the diazonium group expected to introduce a covalent binding between graphene and QDs, thus the small diazonium molecule gives the favorably charge transfer between two components.[34] To form GQ assemblies suitable for light collection and carrier transfer, the linker molecules should be as short as possible to enhance the efficiency of electron tunneling, functionalized to bind the two components and maintain the electronic properties of linked materials. Both graphene and QDs are easily functionalized through both covalent and noncovalent modification. To explore the effect of the non-covalent binding of QDs and graphene on the transport properties, pyridine was chosen as the linker moiety to attach the QDs to graphene. The aromatic pyridine tail allows the nanocrystal to be noncovalently bound to the graphene via π-π stacking interactions (Scheme 1a).[26]

We prepared graphene oxide (GO) by a modified Hummers method.[28] To indicate the acquirement of single-sheet GO, an aqueous solution of GO was dropped into hydrophilic-treated silicon for tapping mode AFM measurements. Figure 2a-b shows an AFM image of GO on the silicon substrate; the thickness of the sheet is equal to or less than 1 nm. Large-area graphene with lateral sizes of more than a few tens of

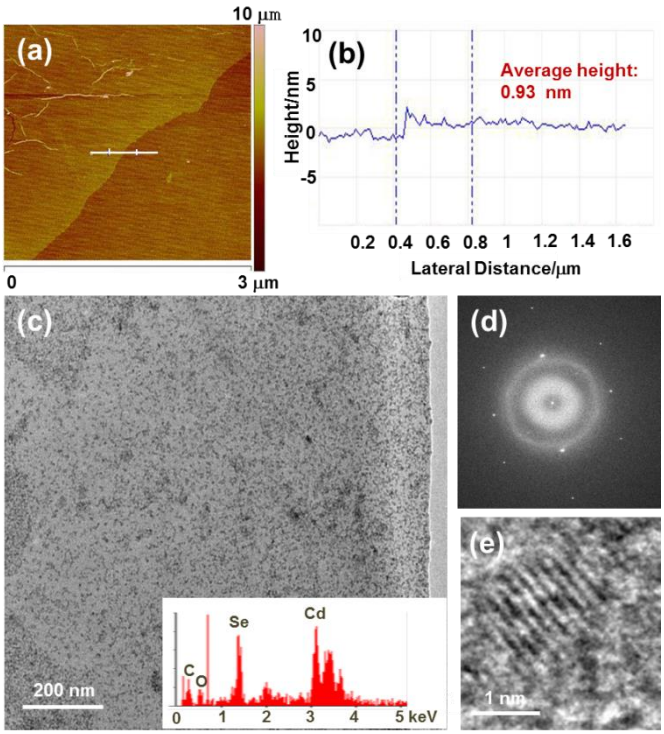

Figure 2. (a) AFM images of single sheet graphene oxide on a silicon substrate, (b) height of single sheet graphene oxide, (c) TEM image of single sheet CdSe aryl binding graphene composite. Inset is the energy dispersive X-ray spectrum confirming the presence of CdSe, (d) The selected area diffraction pattern of CdSe aryl binding graphene composite and (c) The high resolution TEM image of CdSe QDs on graphene.

micrometers can be obtained by low-power ultrasonification and centrifugation. For high-resolution transmission electron microscopy (HR-TEM) sample preparation, a small quantity of GQ composite solution was dropped onto a 300 mesh copper grid. TEM images were obtained from samples attached on the edge of the copper grid, avoiding the complicated lithography process of fabricating a micrometer-sized metallic grid. The lattices of CdSe QDs covering the graphene layer are clearly seen in the high-resolution TEM image (Figure 2c). The individual CdSe nanoparticles with a diameter of ~ 2.8 nm are well separated from each other and spread out on the graphene sheet. There is no aggregation of CdSe QDs on the graphene sheet; nor are large areas of the graphene sheets without CdSe decoration. The good distribution of CdSe QDs on the graphene sheet guarantees efficient optoelectric properties of CdSe QDs. As a result of its efficient electron transport, graphene significantly quenched the fluorescence of the CdSe QDs decorated on it, demonstrating the potential applicability in the field of optoelectronics. The composition of the GQ composites was further confirmed by means of selected area energy dispersive X-ray analysis (SAEDX, see inset image of Figure 2c). The results revealed that the composition was mainly Se, Cd, C and O. Strong signals from Cd and Se suggested the identity of the QDs coupled onto the graphene sheets. The C and O peaks observed in the spectrum could be attributed to the graphene surface. Moreover, the molar ratio of Se to Cd was calculated to be 0.91, approximate to the theoretical value of 1.[35] The selected area diffraction pattern of CdSe aryl binding graphene composite (Figure 2d) and high resolution TEM image of lattices of CdSe QDs covering the graphene layer confirmed the presence of CdSe on graphene (Figure 2e).

We compare the absorbance spectra of graphene, GQ thin films on transparent substrates, and AmTP-capped CdSe QDs in toluene solution. The absorbance peak appearing in the GQ films corresponds to the excitation peak of CdSe QDs, with a small red shift (Figure 3). Previous investigations reported that no QD absorption band could be observed after QDs were attached to CNTs, because the broad background absorption of the CNTs could strongly screen the absorption of the QDs; the absorption band could only been seen when QDs were densely coated onto the CNTs.[36] However, the first excitonic adsorption peak of CdSe in our experiment could still be observed, which suggests the formation of a dense coating of QDs on the graphene sheets. Moreover, no obvious change of the absorption peak of the QDs was observed, which indicates that little or no QDs agglomerates were formed on the graphene sheets,[37] consistent with HR-TEM observations. The PL emission spectrum of GQ composites (Figure 3) shows a dramatic decrease in intensity compared with that of pure QDs, indicating partial quenching. This result can be ascribed to the electron transfer from excited CdSe QDs to graphene.[38] Similar PL quenching was observed in previous reports on CNT–QD composites.[36,39] Furthermore, the nearly constant size distribution of CdSe QDs was verified again by the negligible red shift (1 nm) of the QD band-gap emission after adsorption onto the graphene sheets.[40] The photoluminescence of the QDs

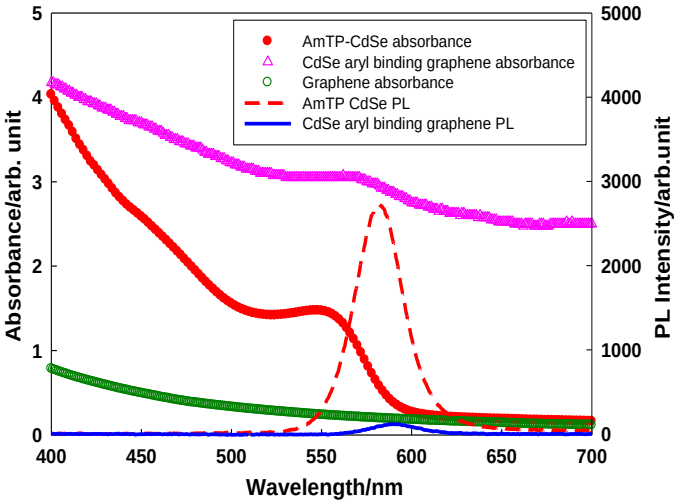

Figure 3. The absorbance and photoluminescence (PL) of CdSe and CdSe aryl binding graphene composite on transparent electrode.

is due to the irradiative pathway from the excited state to the ground state. Given that the graphene quenched the CdSe QDs, the graphene interaction with the QDs must provide an alternative, nonirradiative decay path. It is believed that the nonirradiative decay path occurs because the electron affinity between the CdSe QDs and the graphene is sufficiently small that it allows electron transfer from the QDs to the graphene. In other words, the formation of GQ conjugates favors electron transfer from the QDs (donor) to the graphene (acceptor) such that the excited electrons entered the graphene rather than being emitted as a photoluminescence peak.

Figure 4 shows the Raman spectra of graphene before and after the CdSe aryl radical chemical modification. There are two features in the Raman spectra of graphene, the G mode at ~1585 cm^{-1} and the D mode at ~1350 cm^{-1}. In the CdSe aryl binding graphene, the G mode's position and shape will not change after the chemical modification, implying the reserve of the backbone of the graphene lattice. However, the G mode from the pyridine capping CdSe-graphene was split into two distinct peaks which was fitted wih two Lorentzians peak at ~1589 and 1620 cm^{-1}. because the 2-fold degeneracy of the TO and LO phonons is lifted by symmetry breaking, as found in carbon nanotubes and the aromatic molecule decorated graphene monolayer.[41] But one must have noticed that the most significant change is the appearance of the D mode at ~1350 cm^{-1} in the Raman spectra of modified graphene. The D mode is arising from the defect-involved double resonant Raman process at the K point in the Brillouin zone. In fact, the presence of the D mode is generally used to monitor the covalent bonds formed in graphene and widely accepted.[42] Since the backbone of graphene in the CdSe aryl binding graphene was preserved herein, we successfully modified graphene *via* chemical reaction, and these results prove directly

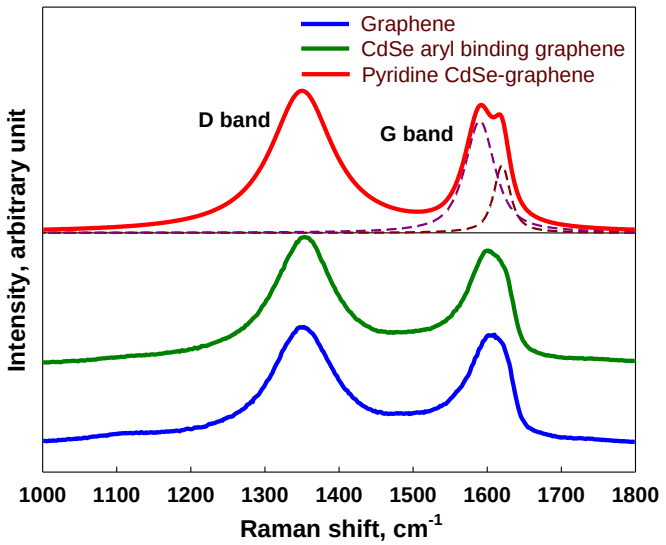

Figure 4. Raman G and D spectra of the CdSe aryl group functionalized graphene layer. Raman spectrum for reference sample, pyridine capping CdSe-graphene and graphene, are also included.

that the appearance of the D mode corresponds to the aryl groups attaching to graphene via σ-bonds.

Time-resolved fluorescence spectroscopy (Figure 5) was employed to monitor the emission lifetimes of free CdSe , pyridine capping CdSe-graphene and CdSe aryl binding graphene. PL decay measurement was accomplished multiple times more than five for each sample. The obtained decay curves were fitted by a three exponential decay model; $I(t) = A_1 e^{-t/\tau_1} + A_2 e^{-t/\tau_2} + A_3 e^{-t/\tau_3}$, where I(t) is the time-dependent fluorescence intensity, A is the amplitude, and τ is the lifetime. The excitation wavelength is 470 nm. Intensity weighted average lifetime, $< \tau_{ave} >$, is defined as $< \tau_{ave} > = \sum_i A_i \tau_i^2 \ / \sum_i A_i \tau_i$. The emission lifetime of pyridine capping CdSe-graphene ($\langle \tau_{ave} \rangle$ = 1.54 ns) nanocrystals was significantly shorter than those of the corresponding CdSe ($\langle \tau_{ave} \rangle$ = 8.8 ns) counterpart (Figure 5a). The difference in the average emission lifetime between GQ and the CdSe counterpart indicates the emergence of a nonradiative pathway from the significant electronic interaction between QDs and graphene. However, as described in Figure 5b, the emission lifetime of CdSe aryl binding graphene ($\langle \tau_{ave} \rangle$ = 0.93 ns) is shorter than that of the pyridine capping CdSe-graphene. Diazonium salts was easily nitrogen loss by either direct photoexcitation or through electron transfer; aryl radicals are thus generated at the graphene surface, where they can react in competition with diffusion into the bulk liquid phase. In the emission quenching process of QDs-graphene system, both electron and energy transfer processes contributed to deactivation of excited CdSe on the graphene surface.[30] The electron transfer from aryl radical functionalized CdSe to graphene surface was expected to be dominated by pathway of the covalent bond. The CdSe aryl radical functionalized graphene could not only accelerate photoinduced electron transfer through the covalent bond but also results in charging of the graphene surface, causing further electron transfer to become increasingly difficult. With the electron transfer pathway unavailable, PL lifetime was increased as energy transfer becomes the only available route for conduction band electrons undergoing nonradiative excited state decay.

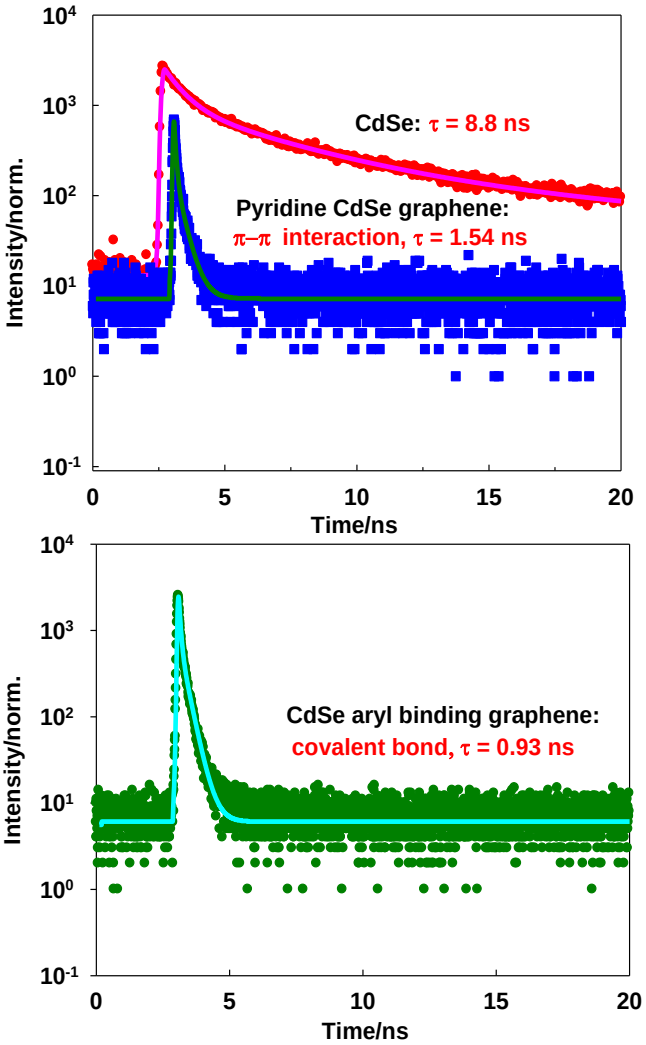

Figure 5. Time-resolved fluorescence spectra of (a) bare CdSe and pyridine capping CdSe-graphene, (b) CdSe aryl binding graphene films on a transparent electrode. The fitting results (solid curves) were also included for comparison.

In order to leverage the benefit of electron transfer observed in GQ composite, the films should contain the balance between the sufficient supply of graphene for ample GQ interfacial contact while also limiting graphene's detrimental filtering of incident light. Film deposition of solution-based composite by means of a spin coating method typically produced in a loss of dispersion between the two species, as well as film inhomogeneity.[30] The previous study reported that the EPD in composite film preparation has been shown to produce films with high quality films.[11,13] By employing an electrophoretic deposition technique, we have cast GQ composite films on a flexible substrate (ITO/PET). When subjected to a DC electric

field, they quickly migrate to the electrode and are deposited on the flexible substrates. The deposition of GQ composite was monitored by UV-vis-NIR absorbance spectroscopy. Absorption spectra show GQ dispersion concentration successively per each cycle until deposition of GQ onto the photoanode is complete. The films obtained by the elecrophoretic deposition method are quite robust, flat film and show homogeneity for spectroscopic and photoelectrochemical measurements. The film of GQ is also highly flexible and more resistive for the bending of film, in contrast to the more fragile dye/TiO_2 system in the DSSCs.

Electronic and optoelectronic characteristics of the devices fabricated from the GQ films on flexible substrates were measured by photocurrent response of ON-OFF illumination. The GQ films were created by electrophoretic deposition. The obtained film thickness is 200 nm. The photoanode is only consisted of QDs and graphene and do not contained the electron transporting layer, such as TiO_2.[30] The film thickness of photoanode is very thin which can be easily applied to flexible solar cells. We constructed cells consisting of GQ composites films as photoanodes with platinum as a counter electrode and aqueous 0.1 M Na_2S as the electrolyte. Upon photoirradation, we observed reproducible responses to ON-OFF light cycles on GQ systems at 100 mW/m^2 and 100 W/m^2 light intensity (Figure 6). The photocurrent response was increased with the light intensity. The photocurrent observed for CdSe aryl radical functionalized graphene (on-off ratio: 28.5) were an order of magnitude higher than the current generated by the pyridine capping CdSe-graphene (on-off ratio: 7.5) at the light intensity of 100 W/m^2. Based on the emission decay result (Figure 5), we expected that CdSe aryl radical functionalized graphene films have the longer charge separation (electron-hole pair). That was caused by the charge trap states which are likely to stabilize the photogenerated charge carriers and contribute to the overall photocurrent generation. Therefore, such longer charge separation is crucial for increasing the probability of charge collection at the electrode surface.[43]

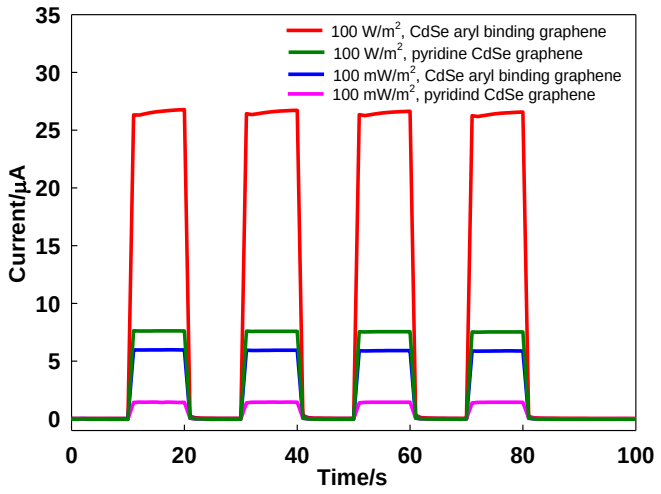

Figure 6. The photocurrent response of the CdSe pyridine and aryl binding graphene films on a flexible electrode to ON-OFF illumination under incident LED light (100 mW/cm^2 and 100 W/cm^2 at 525 nm).

The effect of the dependence of IPCE on the excitation wavelength is shown in Figure 7. The quantum efficiency of CdSe aryl binding graphene was higher than that of the pyridine capping CdSe-graphene even though two hybrid films have the same amount of QDs in the graphene. The enhancement of IPCE in the CdSe aryl binding graphene is attributed to the direct electron transport from the initial excitation of CdSe to the collecting graphene surface. These observations thus confirm that the IPCE response is not only related to the additive effect from the CdSe and graphene components, but rather a result of the unique interactions between the graphene and QDs.[13,44]

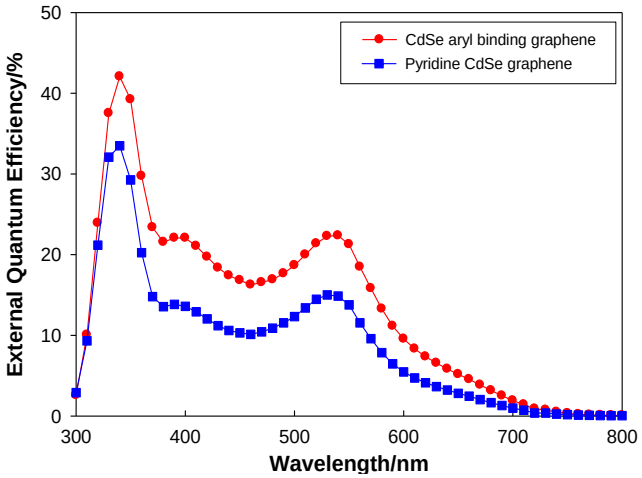

Figure 7. Incident photon to current efficiency (IPCE) of the CdSe pyridine and aryl binding graphene films on a flexible electrode: IPCE (%) = IPCE (λ) = (1240 eV nm)$I_{ph}/\lambda P_0$, where I_{ph} is the incident photocurrent density in mA/cm^2, λ is the wavelength of the incident radiation in nm, and P_0 is the photon flux in mW/cm^2.

The intensity of the IMPS shows (Figure 8a) that the CdSe aryl binding graphene cells have a larger light response than that for pyridine capping CdSe-graphene ones in the measured frequency range, which agrees with the IPCE measurement shown in Figure 7. The inverse of the frequency ($1/2\pi f_{min}$) at the minimum of the IMPS arch represents the typical time interval form photoelectron injection to photoelectrical arrival at ITO/PET electrode. The calculated time interval is 1.97 ms for CdSe aryl binding graphene cells, which is faster than that for pyridine capping CdSe-graphene ones (3.11 ms). Therefore, the photoelectron collection process in covalent GQ composite devices is faster than that in non-covalent GQ composite ones. While IMPS spectra are measured at short-circuit conditions, IMVS spectra are measured at open circuit. Therefore, there is no carrier extraction and IMVS spectra just show accumulation of charge at the interface. The Bode plots of IMVS (Figure 8b) show that the photovoltage of covalent GQ composite devices is higher than that of the non-covalent GQ composite ones as the frequency was decreased. This reflects that electron density of photoanode in covalent GQ composite devices is higher than that in non-covalent GQ composite ones. It increased the quasi

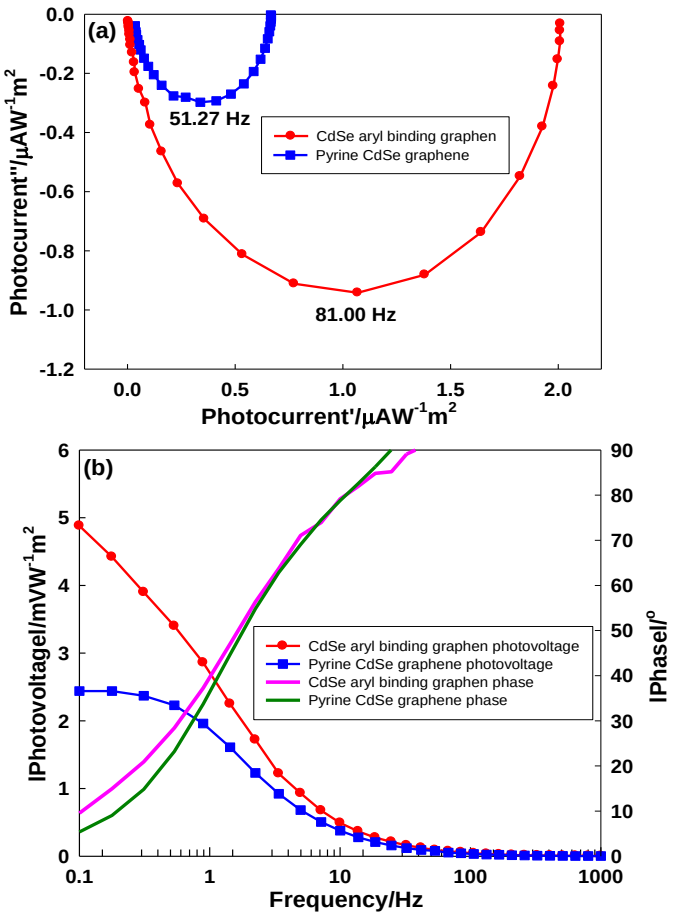

Figure 8. The **(a)** IMPS and (b) Bode diagram of IMVS of GQ composite solar cell with CdSe pyridine and aryl binding graphene

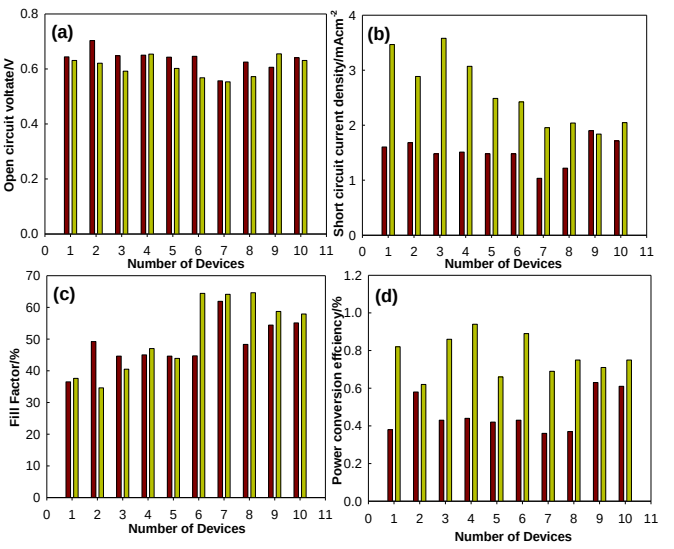

Figure 9. Histogram of device parameters measured for 10 CdSe pyridine(brown color) and aryl binding (green color) graphene composite cells, (a) Voc, (b) Jsc, (c) FF and (d) PCE.

Fermi level of covalent GQ composite devices, resulting in higher photovoltage.

To compare the performance of the covalent and non-covalent GQ composite cells, 10 separate devices were fabricated and tested PV performance. Histograms of the cell-performance characteristics are shown in Figure 9. As can be seen from the results, the Voc (Figure 9a) values show not only highly reproducible but also little difference between covalent and non-covalent graphene-quantum dots composite system. However, the short-circuit current density (Jsc, Figure 9b) and power conversion efficiency (PCE, Figure 9d) of the covalent GQ composite cells higher than that for the non- covalent GQ composite cells. Therefore, we could expect that CdSe aryl radical functionalized graphene could be accelerated photoinduced electron transfer to graphene surface in the competition between charge transfer effect and diffusion into the bulk liquid phase. It led to enhance the photocurrent density and PCE of the composite films. As a result, when the CdSe is directly bound graphene, a large valence band offset will form at graphene/QDs interface while the conduction band offset is very small.[44] Once the photoinduced electrons and holes are generated in the QDs, they will most likely transfer to the graphene owing to the energy band offsets at the interface.[44]

We would acknowlege that low efficiency of the present device is due to the device structure. The photoanode of present device is only consisting of QDs and graphene. The structure of device was different from previous reported devices which involved the TiO_2 to increase the rate of electron transfer.[30] Therefore, although these efficiencies are relatively small, the CdSe aryl binding graphene film could give more useful information between the QDs and graphene interactions to apply the photovoltaic devices.

CONCLUSIONS

In summary, we fabricated composite films via covalent coupling of CdSe QDs to graphene in an aqueous solution. To investigate the carrier transport between CdSe and graphene film, we compared that with the CdSe pyridine capping graphene films which was bound through the π-π interaction between the graphene and pyridine molecule. The Raman spectroscopy result proves that the CdSe aryl groups bond to the graphene basal plane via σ-bonds. The time-resolved fluorescence studies demonstrated that emisson lifetime of CdSe aryl groups binding graphene film is significantly shorter than that of the pyridine capping CdSe-graphene. The quantum efficiency and photocurrent density of CdSe aryl binding graphene were higher than that of the pyridine capping CdSe-graphene. It indicated that , in the competition between charge transfer effect and diffusion into the bulk liquid phase, CdSe aryl radical functionalized graphene could be effectively transported electron to the graphene surface compared to the CdSe pyridine capping graphene films. These results, thus, presented a new route to prepare GQ composite materials, which hold promise as new active or electrode materials in photovoltaic devices.

Acknowledgements
This work was supported by Government funded R&D program under the Ministry of Strategy and Finance, Republic of Korea.

Notes and references
[a] Solar Cell Technology Research Section, IT Components and Materials Industry Technology Research Department, IT Materials and Components Laboratory, Electronics and Telecommunications Research Institute (ETRI), 218 Gajeong-no, Yuseong-gu, Daejeon 305-700, Republic of Korea

1 A. Yella, H.-W. Lee, H. N. Tsao, C. Yi, A. K. Chandiran, M. K. Nazeeruddin, E. W.-G. Diau, C.-Y. Yeh, S. M. Zakeeruddin and M. Grätzel, *Science*, 2011, **334**, 629.
2 J. Burschka, N. Pellet, S.-J. Moon, R. Humphry-Baker, P. Gao, M. K. Nazeeruddin and M. Gratzel, *Nature*, 2013, **499**, 316; M. Liu, M. B. Johnston and H. J. Snaith, *Nature*, 2013, **501**, 395.
3 W.-T. Sun, Y. Yu, H.-Y. Pan, X.-F. Gao, Q. Chen and L.-M. Peng, *J. Am. Chem. Soc.*, 2008, **130**, 1124.
4 I. Robel, V. Subramanian, M. Kuno and P. V. Kamat, *J. Am. Chem. Soc.*, 2006, **128**, 2385.
5 J. H. Bang and P. V. Kamat, *ACS Nano*, 2009, **3**, 1467.
6 S. M. Yang, C. H. Huang, J. Zhai, Z. S. Wang and L. Jiang, *J. Mater. Chem.*, 2002, **12**, 1459.
7 P. Yu, K. Zhu, A. G. Norman, S. Ferrere, A. J. Frank and A. J. Nozik, *J. Phys. Chem. B*, 2006, **110**, 25451; J. S. Kim, J. H. Lee, S. U. Hong, H. S. Kwack and D. K. Oh, *ETRI Journal*, 2004, **26**, 475.
8 W. W. Yu, Y. A. Wang and X. Peng, *Chem. Mater.*, 2003, **15**, 4300.
9 R. D. Schaller and V. I. Klimov, *Phys. Rev. Lett.*, 2004, **92**, 186601.
10 H. J. Lee, J.-H. Yum, H. C. Leventis, S. M. Zakeeruddin, S. A. Haque, P. Chen, S. I. Seok, M. Grätzel and M. K. Nazeeruddin, *J. Phys. Chem. C*, 2008, **112**, 11600.
11 P. Brown and P. V. Kamat, *J. Am. Chem. Soc.*, 2008, **130**, 8890.
12 X. Dang, H. Yi, M. H. Ham, J. Qi, D. S. Yun, R. Ladewski, M. S. Strano, P. T. Hammond and A. M. Belcher, *Nat. Nanotechnol.*, 2011, **6**, 377; T. Hasobe, S. Fukuzumi and P. V. Kamat, *Angew. Chem. Int. Ed.*, 2006, **45**, 755; P. V. Kamat, K. G. Thomas, S. Barazzouk, G. Girishkumar, K. Vinodgopal and D. Meisel, *J. Am. Chem. Soc.*, 2004, **126**, 10757.
13 B. Farrow and P. V. Kamat, *J. Am. Chem. Soc.*, 2009, **131**, 11124.
14 P. V. Kamat, *J. Phys. Chem. C*, 2008, **112**, 18737.
15 I. Robel, B. A. Bunker and P. V. Kamat, *Adv. Mater.*, 2005, **17**, 2458.
16 T. Hasobe, H. Murata and P. V. Kamat, *J. Phys. Chem. C*, 2007, **111**, 16626.
17 X. Geng, L. Niu, Z. Xing, R. Song, G. Liu, M. Sun, G. Cheng, H. Zhong, Z. Liu, Z. Zhang, L. Sun, H. Xu, L. Lu and L. Liu, *Adv. Mater.*, 2010, **22**, 638.
18 H. Hu, B. Zhao, M. A. Hamon, K. Kamaras, M. E. Itkis and R. C. Haddon, *J. Am. Chem. Soc.*, 2003, **125**, 14893.
19 K. Kamaras, M. E. Itkis, H. Hu, B. Zhao and R. C. Haddon, *Science*, 2003, **301**, 1501.
20 M. Delamar, R. Hitmi, J. Pinson and J. M. Saveant, *J. Am. Chem. Soc.*, 1992, **114**, 5883.
21 Y.-C. Liu and R. L. McCreery, *J. Am. Chem. Soc.*, 1995, **117**, 11254.
22 J. L. Bahr, J. Yang, D. V. Kosynkin, M. J. Bronikowski, R. E. Smalley and J. M. Tour, *J. Am.Chem. Soc.*, 2001, **123**, 6536.
23 T. C. Kuo, R. L. McCreery and G. M. Swain, *Electrochem. Solid State Lett.*, 1999, **2**, 288; J. Wang and J. A. Carlisle, *Diamond Relat. Mater.*, 2006, **15**, 279.
24 J. Aldana, Y. A. Wang and X. Peng, *J. Am. Chem. Soc.*, 2001, **123**, 8844.
25 W. Maneeprakorn, M. A. Malik and P. O'Brien, *J. Am. Chem. Soc.*, 2010, **132**, 1780.
26 S. Jeong, H. C. Shim, S. Kim and C.-S. Han, *ACS Nano*, 2009, **4**, 324.
27 N. I. Kovtyukhova, P. J. Ollivier, B. R. Martin, T. E. Mallouk, S. A. Chizhik, E. V. Buzaneva and A. D. Gorchinskiy, *Chem. Mater.*, 1999, **11**, 771.
28 W. S. Hummers and R. E. Offeman, *J. Am. Chem. Soc.*, 1958, **80**, 1339.
29 V. C. Tung, M. J. Allen, Y. Yang and R. B. Kaner, *Nat. Nanotechnol.*, 2009, **4**, 25; D. Li, M. B. Muller, S. Gilje, R. B. Kaner and G. G. Wallace, *Nat. Nanotechnol.*, 2008, **3**, 101.
30 I. V. Lightcap and P. V. Kamat, *J. Am. Chem. Soc.*, 2012, **134**, 7109.
31 Y.-L. Lee and C.-H. Chang, *J. Power Sources*, 2008, **185**, 584.
32 A. T. Overton and A. A. Mohamed, *Inorg. Chem.*, 2012, **51**, 5500.
33 M. D. Obushak, M. B. Lyakhovych and M. I. Ganushchak, *Tetrahedron Lett.*, 1998, **39**, 9567.
34 Q. Li, B. Sun, I. A. Kinloch, D. Zhi, H. Sirringhaus and A. H. Windle, *Chem. Mater.*, 2006, **18**, 164.
35 Y. Zheng, Z. Yang and J. Y. Ying, *Adv. Mater.*, 2007, **19**, 1475.
36 M. Grzelczak, M. A. Correa-Duarte, V. Salgueiriño-Maceira, M. Giersig, R. Diaz and L. M. Liz-Marzán, *Adv. Mater.*, 2006, **18**, 415.
37 B. Pan, D. Cui, C. S. Ozkan, M. Ozkan, P. Xu, T. Huang, F. Liu, H. Chen, Q. Li, R. He and F. Gao, *J. Phys. Chem. C*, 2008, **112**, 939.
38 A. Cao, Z. Liu, S. Chu, M. Wu, Z. Ye, Z. Cai, Y. Chang, S. Wang, Q. Gong and Y. Liu, *Adv. Mater.*, 2010, **22**, 103.
39 Q. Li, B. Sun, I. A. Kinloch, D. Zhi, H. Sirringhaus and A. H. Windle, *Chem. Mater.*, 2005, **18**, 164.
40 C. Nethravathi, T. Nisha, N. Ravishankar, C. Shivakumara and M. Rajamathi, *Carbon*, 2009, **47**, 2054.
41 P. Huang, H. Zhu, L. Jing, Y. Zhao and X. Gao, *ACS Nano*, 2011, **5**, 7945.
42 D. C. Elias, R. R. Nair, T. M. G. Mohiuddin, S. V. Morozov, P. Blake, M. P. Halsall, A. C. Ferrari, D. W. Boukhvalov, M. I. Katsnelson, A. K. Geim and K. S. Novoselov, *Science*, 2009, **323**, 610; R. Sharma, J. H. Baik, C. J. Perera and M. S. Strano, *Nano Lett.*, 2010, **10**, 398; H. Liu, S. Ryu, Z. Chen, M. L. Steigerwald, C. Nuckolls and L. E. Brus, *J. Am. Chem. Soc.*, 2009, **131**, 17099; S. Niyogi, E. Bekyarova, M. E. Itkis, H. Zhang, K. Shepperd, J. Hicks, M. Sprinkle, C. Berger, C. N. Lau, W. A. deHeer, E. H. Conrad and R. C. Haddon, *Nano Lett.*, 2010, **10**, 4061; K. N. Kudin, B. Ozbas, H. C. Schniepp, R. K. Prud'homme, I. A. Aksay and R. Car, *Nano Lett.*, 2007, **8**, 36.
43 S. Barazzouk, S. Hotchandani, K. Vinodgopal and P. V. Kamat, *J. Phys. Chem. B*, 2004, **108**, 17015.
44 Y. Lin, K. Zhang, W. Chen, Y. Liu, Z. Geng, J. Zeng, N. Pan, L. Yan, X. Wang and J. G. Hou, *ACS Nano*, 2010, **4**, 3033.